Electronic Supplementary Material (ESI) for Journal of Materials Chemistry A.

Supplementary Information

High Performance Fiber-shaped Supercapacitors Based on Core-shell Fiber Electrodes with Adjustable Surface Wrinkles and Robust Interfaces

Hang Shi, Song Chen*, Wei Shi, Zefei Peng, Junyun Li, Zelin Liu, Guangyong Zhang, Lan Liu*

College of Materials Science and Engineering, Key Lab of Guangdong Province for High Property and Functional Macromolecular Materials, South China University of Technology, Guangzhou, 510641, P. R. China

S1-S2 Optical photos of polymerization of PPy

S1

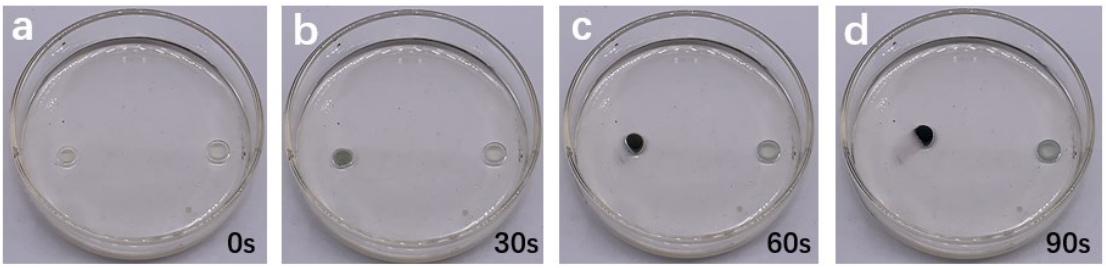

Fig. S1 PPy polymerization rate comparison of different initiator solution: mixture solution of $FeCl_3$ and Na-PTS (the left drop) and pure $FeCl_3$ solution (the right drop) react with Py monomer for (a) 0s, (b) 30s, (c) 60s and (d) 90s.

Comparing the two drops, it can be seen clearly that the mixture solution of $FeCl_3$ and Na-PTS reacts faster with Py monomers than pure $FeCl_3$ solution.

S2 the GO/Alg/PPy gel fibers reacted with Py monomers for 30s, 60s and 90s, and after drying and reduction, the rGO/Alg/PPy was marked as 20G/30s, 20G/60s and 20G/90s, respectively.

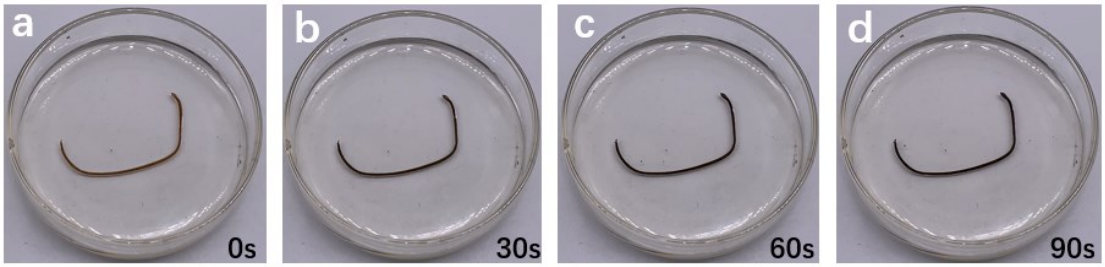

Fig. S2 Optical photos of the GO/Alg/PPy gel fiber reacts with Py monomers for (a)0s, (b)30s, (c)60s and (d)90s after immersing in Solution A for 60s.

With the increasing of reaction time, the color of fiber surface turned into deep black gradually, indicating that the longer reaction time was, the more PPy produced on the surface of fiber. And because of the growth of PPy content, 20G/90s shows largest capacitance among the three.

S3-S6 Characterization of rGO/Alg/PPy fiber

S3 Optical photos of the fiber profile

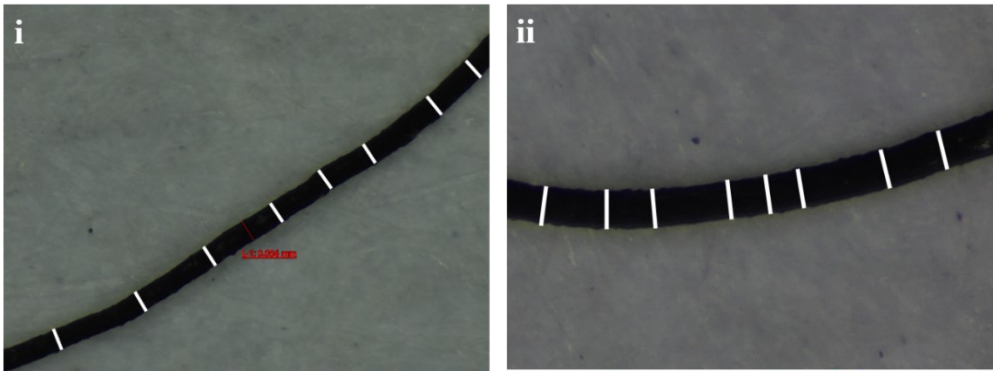

Fig. S3 Optical photo of fiber profile (the white scale bar = 0.056mm).

During the wet-spinning and preparation of our fibers, we controlled the process strictly and the rGO/Alg/PPy fibers are formation after air drying and reduction and these two procedures, which may cause the small defects of the fiber profile. However, relatively uniform rGO/Alg/PPy fibers was still obtained.

S4

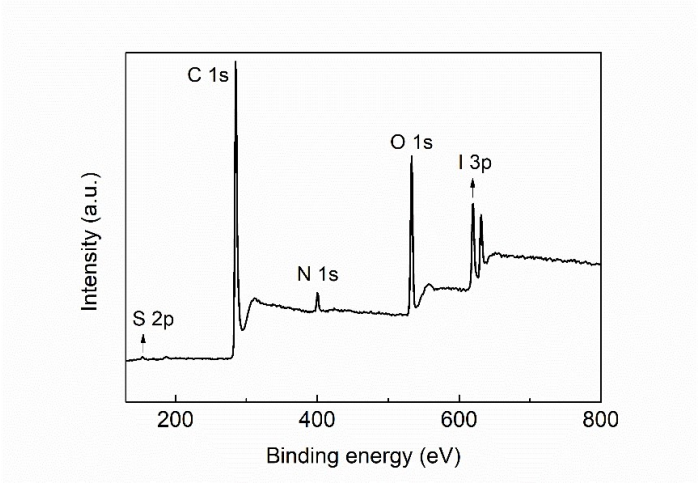

Fig. S4 XPS survey spectrum of rGO/Alg/PPy fiber

The XPS survey spectrum shows the presence of C, O, N, I, and S elements.

S5 EDS line scanning of at the edge of rGO/Alg/PPy fiber.

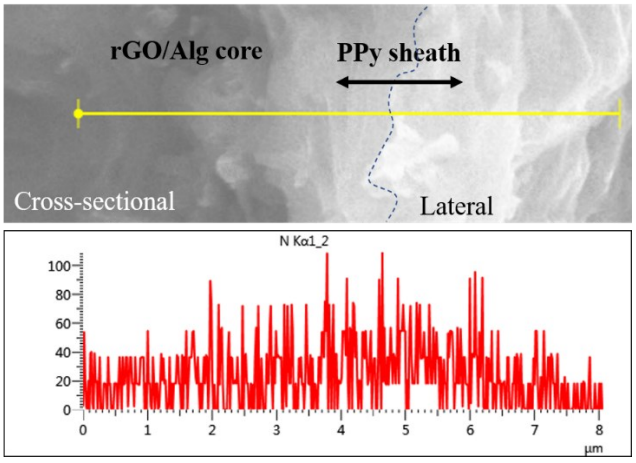

Fig. S5 EDS line scanning at the fiber edge.

In order to confirm the permeation of PPy in Alg, we carried out the EDS line scanning at the fiber edge. The Fig. S5 shows that the distribution of N elements increases along the direction of core to sheath at the edge.

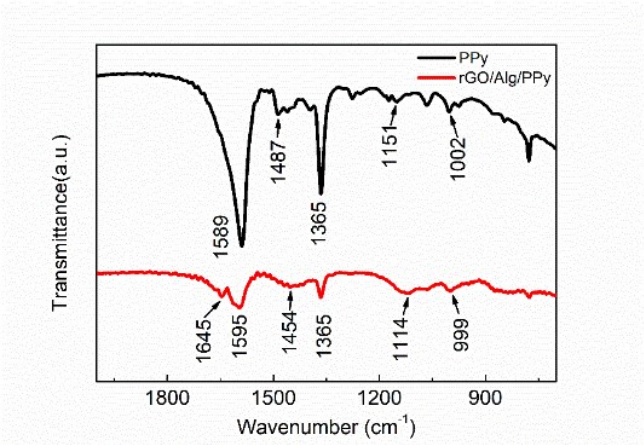

Fig. S6 FTIR spectra of pure PPy and rGO/Alg/PPy fiber

In the FTIR spectrum of PPy, the bands at 1595 and 1454 cm^{-1} are attributed to the pyrrole ring vibration. The bands located at 1365 is ascribed to vibrations of C-H bond. Other bands at 1114 and 999 cm^{-1} indicate the formation of doped PPy. However, in the FTIR spectrum of rGO/Alg/PPy fiber, the peaks around 1645 cm^{-1} are attributed to asymmetric stretching vibrations of $-COO^-$ of Alg and the main characteristic peaks of PPy are red-shifted which demonstrates the strong interactions between PPy sheath and the rGO/Alg core.[1-4]

S7-S9 rGO/Alg fibers were obtained by directly reduced from GO/Alg fibers wet-spun through 20G nozzle and the morphology, composition and electrochemical performances of rGO/Alg fibers were analyzed.

S7

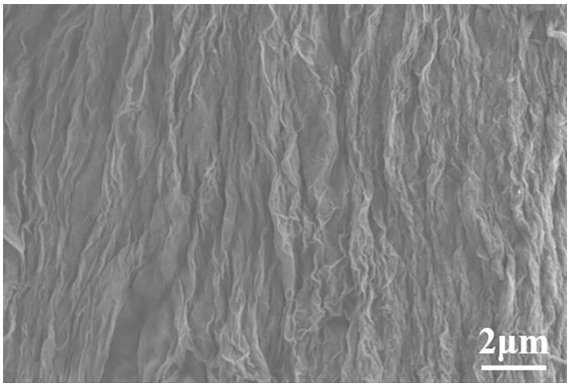

Fig. S7 SEM image of the surface of rGO/Alg fiber.

The surface of rGO/Alg fiber shows the common wrinkles that occurs on the surface of rGO-based fibers. These wrinkles are obviously different from the PPy wrinkles of rGO/Alg/PPy core-shell fibers.

S8

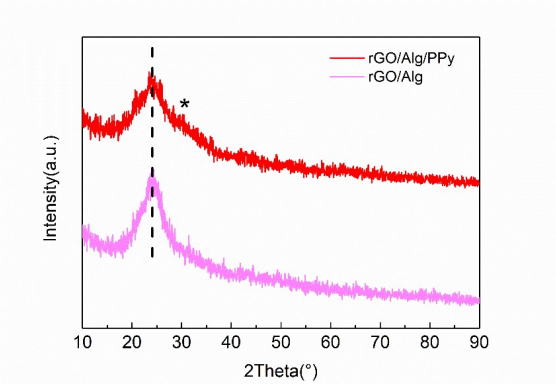

Fig. S8 XRD curves of rGO/Alg/PPy and rGO/Alg fibers

The XRD curve of rGO/Alg fiber shows a peak of rGO at around 24°, while the curve of rGO/Alg/PPy shows a broader peak which derives from the overlap of peaks of rGO and amorphous PPy[5].

S9 Comparison of electrochemical performance of 20G/90s and rGO/Alg fibers.

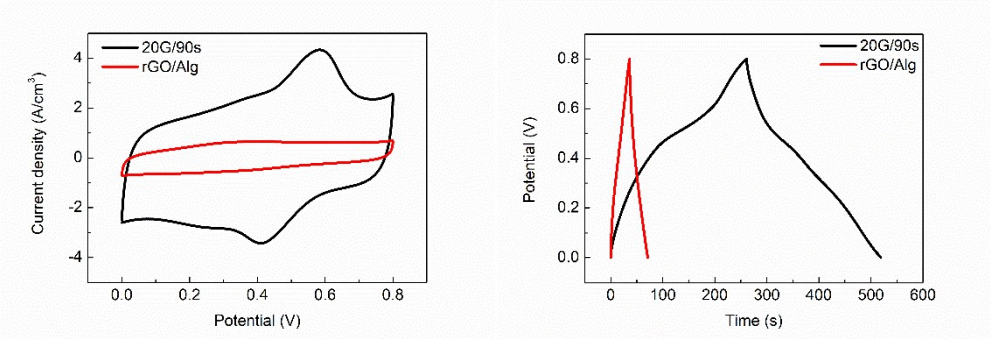

Fig. S9 Electrochemical performance comparison between 20G/90s and rGO/Alg fibers. (a) CV curves at scan rate of 10 mV/s, (b) GCD curves at current density of 1 A cm^{-3}.

S10-S11 Surface morphology analyses of 20G/90s, 18G/90s and 16G/90s fibers and mechanical tests of fibers.

S10

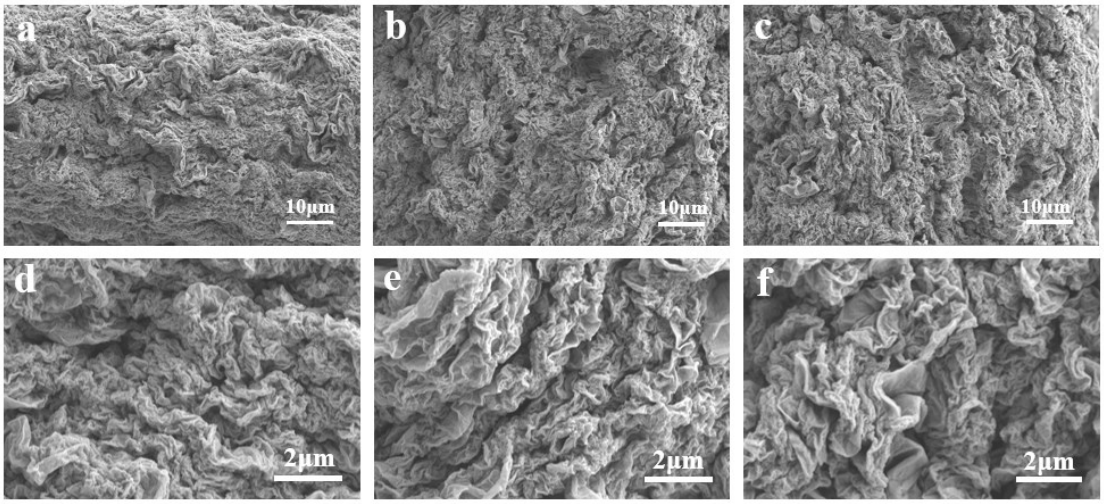

Fig. S10 SEM images of rGO/Alg/PPy fibers of different shrinkage ratios. Surface view of (a) 20G/90s, (b) 18G/90s and (c) 16G/90s. Enlarged surface views of (d) 20G/90s, (e) 18G/90s and (f) 16G/90s.

S11

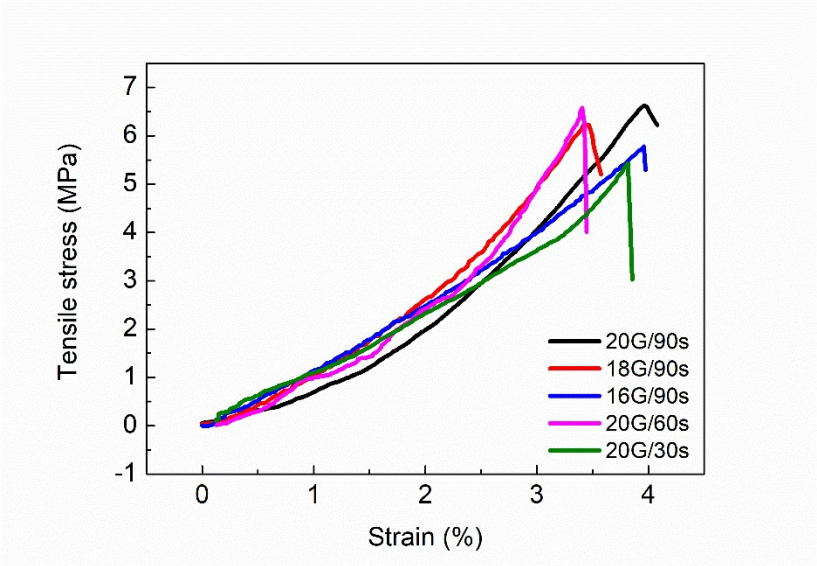

Fig. S11 Tensile stress–strain curves of different fibers.

Although the fibers have different diameters and PPy content, they show similar mechanical performances and the tensile-stress are measured to be about 6 MPa. In fact, with the increase of fiber diameter, the fiber become brittle, and the tensile strength is affected slightly. Besides, even if the reaction time is prolonged to 90s, the PPy sheath is too thin to influence the tensile strength of the whole fiber.

S12 Comparison of 20G/120s and 20G/90s in electrochemical properties.

20G/120s fiber was obtained by prolonging the reaction time to 120s.

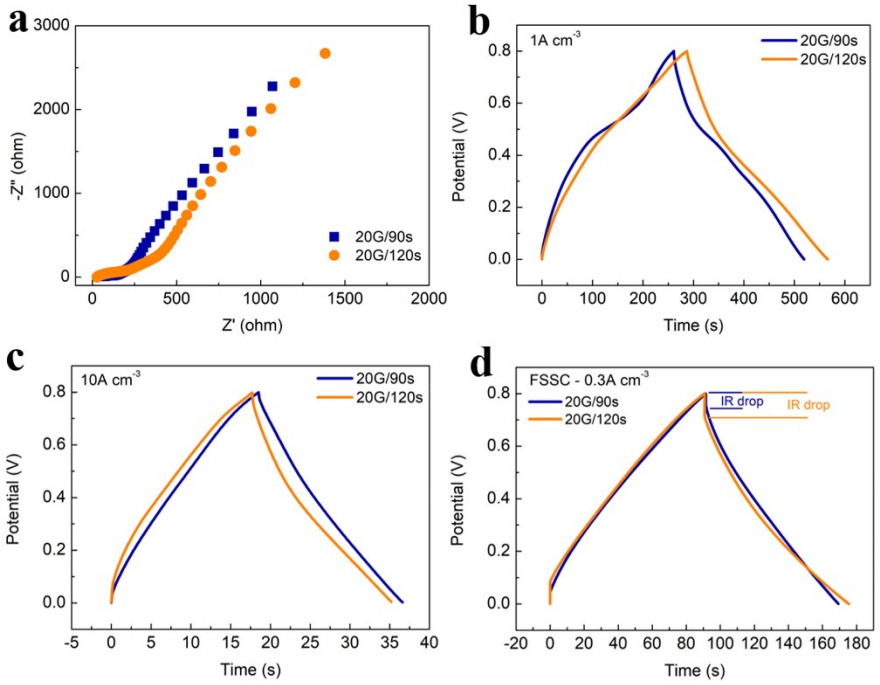

Fig. S12 (a) EIS curves of 20G/90s and 20G/120s fibers. (b) GCD curves of 20G/90s and 20G/120s as a single electrode at current density of 1A cm^{-3}. (c) GCD curves of 20G/90s and 20G/120s as a single electrode at current density of 10A cm^{-3}. (d) GCD curves of FSSCs fabricated by 20G/90s and 20G/120s fibers at current density of 0.3 A cm^{-3}.

The EIS curves (Fig. S12a) shows that 20G/120s fiber possesses higher resistance than 20G/90s fiber. And the GCD curves (Fig. S12b) show that the discharging time of 20G/120s fiber is slightly longer than that of 20G/90s at the current density of 1A cm^{-3}, and when the current density is increased to 10 A cm^{-3}, the discharging time of 20G/120s fiber decreases more than 20G/90s, indicating worse rate capability of 20G/120s (Fig. S12c).

It is worth noting that the PPy content of fiber will not infinitely increase with the extension of reaction time with Py monomers, on the contrast, it is also restricted by the amount of Fe^{3+} absorbed when the gel GO/Alg fiber was immersed in $FeCl_3$ and Na-PTS solution. And in our work, when the reaction time is within 90 seconds, the PPy content increased obviously. However, it is supposed that the PPy content just increased slightly when prolonging the reaction time with Py monomer to 120 seconds. Although the increase of PPy is good for the specific capacitance, it has passive influence on the resistance of fibers. And this influence further reflected by the larger IR drop in GCD curves (Fig. S12d) when the two kinds of fibers were fabricated into FSSCs. In conclusion, taking all the factors into consideration, 90 seconds is the better reaction time because of the large specific capacitance, good rate capability, low resistance of 20G/90s fibers and small IR drop of FSSC.

S13-S16 Preparation and characterization of wrinkle-free rGO/Alg/PPy (rGO/Alg/WF-PPy) fibers.

S13 Preparation of wrinkle-free rGO/Alg/PPy (rGO/Alg/WF-PPy) fiber

For preparing rGO/Alg/WF-PPy fiber: Using the same method, GO/Alg gel fibers were obtained and then dried on a clean weighing paper at ambient temperature. Next, the dried GO/Alg fibers were immersed in solution A for 10 minutes and immediately picked up and immersed in Py monomer for 90s to obtain wrinkle-free GO/Alg/PPy fibers, followed by washing with ethanol and deionized water. The dried GO/Alg/PPy fibers were put into 40% HI acid for 8h at 80 ℃ for reduction to form rGO/Alg/WF-PPy fibers.

S14

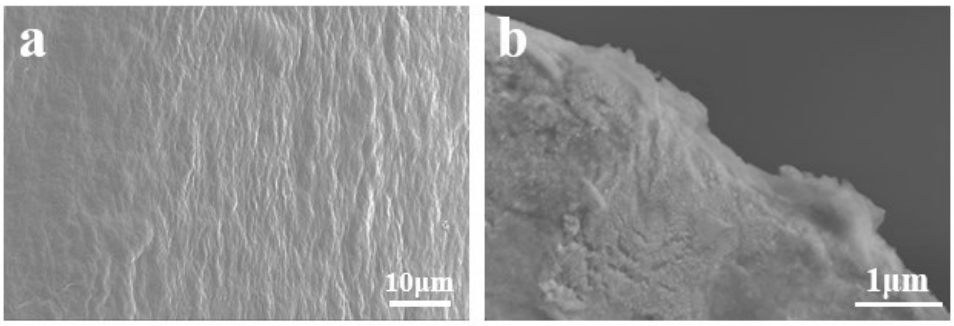

Fig. S14 Morphology characterization of wrinkle-free rGO/Alg/PPy (rGO/Alg/WF-PPy) fiber. (a) Enlarged cross section view of rGO/Alg/WF-PPy fiber edge. (b) Surface view of rGO/Alg/WF-PPy fiber.

The rGO/Alg/WF-PPy fibers were prepared by adjusting the sequences of preparation procedures. It is the volume shrinkage of the gel fibers that drives the PPy sheath to form wrinkles, so drying the gel fibers before the formation of PPy sheath ultimately results in the plane surface of PPy.

S15

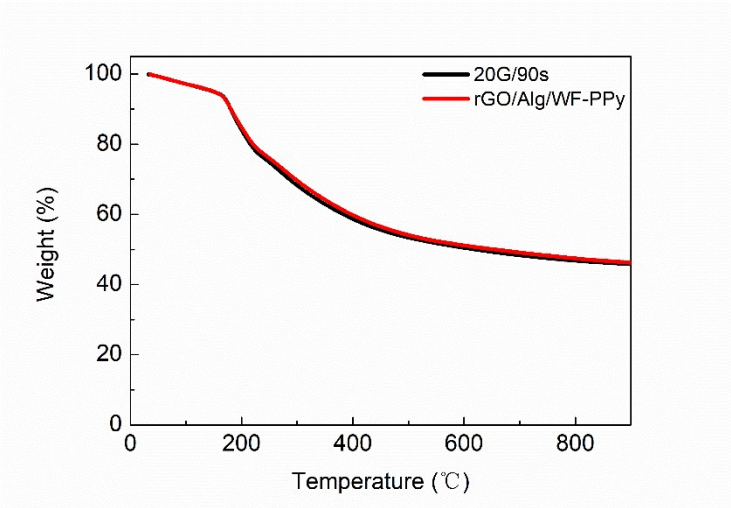

Fig. S15 TG curves of 20G/90s and rGO/Alg/WF-PPy fiber.

The TG curve of rGO/Alg/WF-PPy fibers shows almost identical weight-loss behaviors and weight retention with 20G/90s fibers. Since the initial ratio of GO and alginate is constant, the content of PPy can be rationally speculated to be the same. The only difference between rGO/Alg/WF-PPy fibers and 20G/90s fibers is the specific superficial areas.

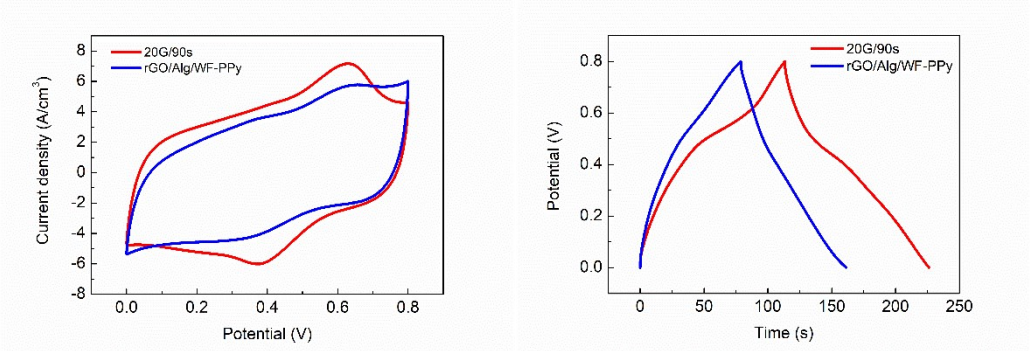

Fig. S16 Electrochemical performance comparison between 20G/90s and rGO/Alg/WF-PPy fiber. (a) CV curves at scan rate of 20 mV/s, (b) GCD curves at current density of 2 A cm^{-3}.

The CV curves of rGO/Alg/WF-PPy fibers and 20G/90s fibers show the wrinkled 20G/90s fibers with larger superficial area possess higher specific capacitance. The GCD curves display that the wrinkled 20G/90s fibers have longer discharging time demonstrating better electrochemical performance. It is worth noting that the more distinct redox peaks in the CV and GCD curves of 20G/90s fibers are also attributed to the large superficial area which permits more charge to reach on the surface to proceed sufficient redox reactions.

S17 Contribution of capacitance

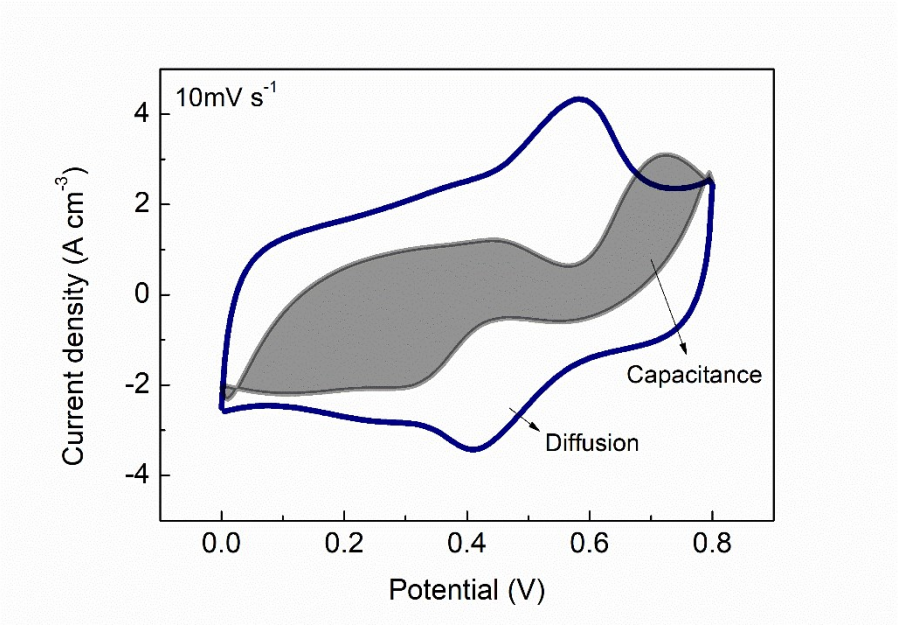

Fig. S17 Contribution of capacitance at the scan rate of 10mV s^{-1}.

Capacitance contribution from capacitive and diffusion-controlled process of the 20G/90s fiber at the scan rate of 10mV s^{-1} is showed in Fig. S17, and the contribution of capacitance is calculated as 57.73%.

S18 Equivalent circuit for EIS

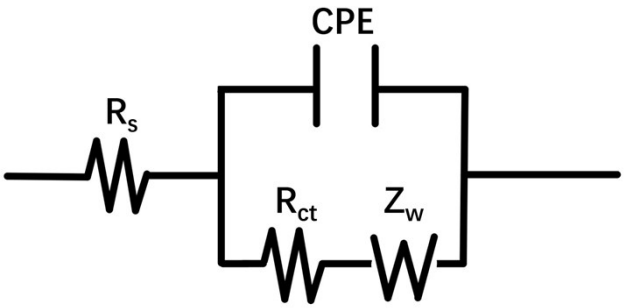

Fig. S18 equivalent circuit for EIS.

S19 Electrochemical performance calculations:

The volume of fiber was calculated by considering the fiber as a cylinder. In every electrochemical test, five diameters at different positions of the fiber electrode were measured by a thickness gauge and SEM, and the final diameter was the average of these five data. And the volume of fiber was calculated according to the following equation:

$$V_d = \pi\left(\frac{d}{2}\right)^2 \tag{1}$$

where the V_d (cm^3) is the volume of fiber electrode, and d (cm) is the final diameter.

The volumetric capacitance of fiber electrode (C_V, F cm^{-3}), volumetric capacitance of FSSC device (C_D, F cm^{-3}), volumetric energy density (E_V, mWh cm^{-3}) and volumetric power density (P_V, mW cm^{-3}) were calculated according to the following equations:

$$C_V = \frac{2I \cdot T}{V_E \cdot U} \tag{2}$$

$$C_D = \frac{2I \cdot T}{V_D \cdot U} \tag{3}$$

$$E_V = \frac{C_D \cdot U^2}{2 \cdot 3.6} \tag{4}$$

$$P_V = \frac{3.6E_V}{t} \tag{5}$$

where I (A) is the discharge current, T (s) is the discharge time from GCD curves, V_E (cm^3) is the volume of the fiber electrode, V_D (cm^3) is the volume of the supercapacitor and U (V) is the corresponding potential window from GCD curves.

S20 Calculation method of Table S1

Assuming the GO/Alg/PPy gel fiber is an ideal cylinder and the PPy sheath is a hollow cylinder, the calculation methods should be as follows:

- A GO/Alg/PPy gel fiber is prepared and the length is measured as L_0. After drying and reducing this gel fiber, the obtained rGO/Alg/PPy fiber is measured as L_1 long. Length shrinkage ratio (r_L) is calculated from the the equation:

$$r_L = \frac{L_0}{L_1} \tag{6}$$

  It is worth noting that in the shrinkage process the PPy sheath will maintain its original volume and superficial area despite the formation of wrinkles.

- Superficial area of PPy sheath (S_A, mm^2) is calculated from equation:

$$S_A = 10\pi \cdot r_L \cdot (D_N + 2T_{PPy}) \tag{7}$$

  where S_A is the superficial area of PPy sheath, r_L is the length shrinkage ratio, D_N is the diameter of nozzle and T_{PPy} is the thickness of PPy sheath and it can be inferred from SEM images that T_{PPy} is about 0.1 μm.

- Volume of PPy (V_{PPy}, mm^3) is calculated from equation:

$$V_{PPy} = 10\pi \cdot r_L \cdot T_{PPy}(D_N + T_{PPy}) \tag{8}$$

  where V_{PPy} is volume of PPy, r_L is the length shrinkage ratio, T_{PPy} is the thickness of PPy sheath and D_N is the diameter of nozzle.

- Diameter of dried rGO/Alg/PPy fiber (D_F, mm) is the average diameter of 3 fibers measured by a thickness gauge.

- Volume of dried rGO/Alg/PPy fiber (V_F, mm^3) is calculated from equation:

$$V_F = 10\pi \cdot r_L \left(\frac{D_F}{2}\right)^2 \tag{9}$$

  where V_F is Volume of dried rGO/Alg/PPy fiber, r_L is the length shrinkage ratio and D_F is diameter of dried rGO/Alg/PPy fiber.

- Relative content of PPy (C_{PPY}) is calculated from equation:

$$C_{PPy} = \frac{V_{PPy}}{V_F} \times 100\% \tag{10}$$

  where C_{PPy} is relative content of PPy, V_{PPy} is volume of PPy and V_F is Volume of dried rGO/Alg/PPy fiber.

- Specific superficial area (S_v, mm^{-1}) is calculated from equation:

$$S_V = \frac{S_A}{V_F} \tag{11}$$

  where S_v is specific superficial area, S_A is the superficial area of PPy sheath and V_F is Volume of dried rGO/Alg/PPy fiber.

Table S1 Theoretical calculation of composition content of rGO/Alg/PPy fibers in a certain length (every 10 mm)

Diameter of nozzle (mm)	Length shrinkage ratio	Superficial area of PPy sheath (mm^2)	Volume of PPy (mm^3)	Diameter of rGO/Alg/PPy fiber (mm)	Volume of rGO/Alg/PPy fiber (mm^3)	Relative content of PPy	Specific superficial area (mm^{-1})
0.6	2.00	37.712	0.00377	0.056	2.463×10^{-3}	1.531	1.531×10^{4}
0.8	1.90	47.764	0.00477	0.083	5.411×10^{-3}	0.882	8.827×10^{3}
1.2	1.78	67.116	0.00671	0.115	1.039×10^{-2}	0.646	6.459×10^{3}

Table S2 Simulated Equivalent circuit parameters

Fibers	R_s (ohm)	R_{ct} (ohm)	CPE (10^{-7}F)	Z_w ($S \cdot sec^{0.5}$)	χ^2
20G/30s	25.44	17.42	7.720	0.001861	0.09713
20G/60s	30.64	24.16	15.99	0.001879	0.09181
20G/90s	77.19	123.2	11.49	0.000707	0.07202
18G/90s	17.72	36.03	8.507	0.001513	0.12480
16G/90s	14.54	16.58	20.36	0.002900	0.09535
rGO/Alg /WF-PPy	71.95	159.7	7.468	0.000536	0.06211

The simulated equivalent circuit is shown in Fig. S11, where R_s is the equivalent series resistance; R_{ct} is interfacial charge transfer resistors in the surface of electrolyte/electrode. Warburg impedance Z_w reflects ion diffusion/transport at the electrode/electrolyte interface and constant phase element. CPE is associated with the double-layer capacitance considering the actual morphology of microfibers.

Table S3 Comparison of electrochemical properties of FSSCs

Serial number	Electrode materials	Specific capacitance of electrode	Specific capacitance of FSSC	Energy density at power density	Reference
1	rGO/Alg/PPy	326.20 F cm^{-3} at 1 A cm^{-3}	36.36 F cm^{-3} at 0.1 A cm^{-3}	2.93 mWh cm^{-3} at 40.8 mW cm^{-3}; 2.15 mWh cm^{-3} at 493.6 mW cm^{-3}	This work
2	cellulose nanofibers/graphene@ polypyrrole microfibers	960F cm^{-3} at 0.1A cm^{-2}	862F cm^{-3} at 0.1A cm^{-2}	19.16 mWh cm^{-3} at 26.67 mW cm^{-3}	S6
3	PEDOT/polypyrrole fibers	478.5 F cm^{-3} at 2A cm^{-3}	-	8.3 mWh cm^{-3} at 389.1 mW cm^{-3}	S7
4	polypyrrole/carbon fiber	-	14.8 F cm^{-3}	2.7 mWh cm^{-3} at power density of 0.029W cm^{-3}	S8
5	carbon nanotube/polypyrrole and hydroquinone	-	42 F cm^{-3}	3.6 mW h cm^{-3} at 59 mW cm^{-3}; 2.9 mW h cm^{-3} at 281 mW cm^{-3}	S9
6	nano-RuO_2-decorated holey graphene	1054 F cm^{-3} at 2 mV s^{-1}	196 F cm^{-3} at 300 mA cm^{-3}	27.3 mWh cm^{-3} at 147.7 mW cm^{-3}; 15.9 mW cm^{-3} at 2954.1 mW cm^{-3}	S10
7	graphene (coaxial fiber-shaped graphene@PVDF nanofiber@ graphene supercapacitor)	-	35.5 F cm^{-3} at 0.6 mA cm^{-2}	3.1 mWh cm^{-3} at 24.2 mW cm^{-3}; 1.8 mWh cm^{-3} at 400.1 mW cm^{-3}	S11

Table S4 Cycling stability

Serial number	Electrode material	Electrolyte	Cycle number	Current density/Scan rate	Capacitance rentention	Reference
1	reduced graphene oxide/alginate/polypyrrole	1M H_2SO_4	10000	10A cm^{-3}	91.61%	This work
	reduced graphene oxide/alginate/polypyrrole	PVA/H_2SO_4 gel	10000	500mA cm^{-3}	80.93%	
2	PEDOT/polypyrrole fibers	PVA/H_2SO_4 gel	10000	5 A cm^{-3}	71.4%	S7
3	cellulose nanofibers/graphene@ polypyrrole microfibers	1M H_2SO_4	10000	1 mA cm^{-2}	96.2%	S6
4	reduced graphene oxide/polypyrrole	PVA/H_2SO_4 gel	10000	3 mA cm^{-2}	73.2%	S12
5	carbon nanotube/polypyrrole and hydroquinone	PVA/H_2SO_4 gel	2000	1A g^{-1}	103%	S9
6	polypyrrole/carbon fiber	LiCl/PVA gel	5000	200 mV s^{-1}	85%	S8
7	polypyrrole/dodecyl benzene sulfonate/ carbon fiber	$LiClO_4$/PVA	5000	100 mV s^{-1}	80.1 %	S13
8	GO/CNTs-TPU fiber	H_2SO_4 solution	8000	100 mV s^{-1}	97.7%	S14
9	Carbon fibers/carbon nanotubes/polypyrrole (asymmetric)	PVA/H_3PO_4 gel	10000	/	more than 90%	S15
10	polypyrrole	PVA/H_3PO_4 gel	10000	/	≈80%	S16

References:

S1 M.A. Guo-Fu, M.U. Jing-Jing, Z. Zhi-Guo, S. Kan-Jun, P. Hui and L. Zi-Qiang, 2013, **29**, 2385-2391.

S2 Y. Shi, L. Pan, B. Liu, Y. Wang, Y. Cui, Z. Bao and G. Yu, *J. Mater. Chem. A*, 2014, **2**, 6086-6091.

S3 J. Zhang and X.S. Zhao, *The Journal of Physical Chemistry C*, 2012, **116**, 5420-5426.

S4 X. Zhang, H. Li, W. Zhang, Z. Huang, C.P. Tsui, C. Lu, C. He and Y. Yang, *Electrochim. Acta*, 2019, **301**, 55-62.

S5 D. Zhang, X. Zhang, Y. Chen, P. Yu, C. Wang and Y. Ma, *J. Power Sources*, 2011, **196**, 5990-5996.

S6 M. Chen, B. Wu and D. Li, *Macromol. Mater. Eng.*, 2020, **305**, 1900854.

S7 W. Teng, Q. Zhou, X. Wang, H. Che, P. Hu, H. Li and J. Wang, *Chem. Eng. J.*, 2020, **390**, 124569.

S8 W. Yuan, G. Han, Y. Xiao, Y. Chang, C. Liu, M. Li, Y. Li and Y. Zhang, *Appl. Surf. Sci.*, 2016, **377**, 274-282.

S9 R. Xu, F. Guo, X. Cui, L. Zhang, K. Wang and J. Wei, *J. Mater. Chem. A*, 2015, **3**, 22353-22360.

S10 S. Zhai, C. Wang, H.E. Karahan, Y. Wang, X. Chen, X. Sui, Q. Huang, X. Liao, X. Wang and Y. Chen, *Small*, 2018, **14**.

S11 Z. Yang, Y. Jia, Y. Niu, Z. Yong, K. Wu, C. Zhang, M. Zhu, Y. Zhang and Q. Li, *Chem. Eng. J.*, 2020, **400**, 125835.

S12 X. Guo, N. Bai, Y. Tian and L. Gai, *J. Power Sources*, 2018, **408**, 51-57.

S13 W. Zhou, G. Han, Y. Xiao, Y. Chang, W. Yuan, Y. Li, C. Liu and Y. Zhang, *Electrochim. Acta*, 2015, **176**, 594-603.

S14 G. Wu, X. Yang, J. Li, N. Sheng, C. Hou, Y. Li and H. Wang, *Chinese J. Polym. Sci.*, 2020, **38**, 531-539.

S15 J. Liu, X. Xu, J. Yu, J. Hong, C. Liu, X. Ouyang, S. Lei, X. Meng, J. Tang and D. Chen, *Electrochim. Acta*, 2019, **314**, 9-19.

S16 L. Li, Z. Lou, D. Chen, W. Han and G. Shen, *Advanced Materials Technologies*, 2018, **3**, 1800115.